Microphysical Simulation of the 2022 Hunga Volcano Eruption Using a Sectional Aerosol Model

Chenwei Li, Yifeng Peng, Elizabeth Asher, Alexandre Baron, Michael Todt, Troy Thornberry, Stéphanie Evan, Jerome Brioude, Penny Smale, Richard Querel, et al.

AGU ADVANCING EARTH AND SPACE SCIENCES

Geophysical Research Letters®

RESEARCH LETTER
10.1029/2024GL108522

Microphysical Simulation of the 2022 Hunga Volcano Eruption Using a Sectional Aerosol Model

Chenwei Li[1,2], Yifeng Peng[3], Elizabeth Asher[4,5], Alexandre A. Baron[5,6], Michael Todt[5,6,7], Troy D. Thornberry[6], Stephanie Evan[8], Jerome Brioude[8], Penny Smale[9], Richard Querel[9], Karen H. Rosenlof[6], Luxi Zhou[10], Jingyuan Xu[11], Kai Qie[11], Jianchun Bian[11], Owen B. Toon[12], Yunqian Zhu[5,6], and Pengfei Yu[1,2]

[1]Institute for Environmental and Climate Research, College of Environment and Climate, Jinan University, Guangzhou, China, [2]Guangdong-Hong Kong-Macau Joint Laboratory of Collaborative Innovation for Environmental Quality, Guangzhou, China, [3]College of Atmospheric Sciences, Lanzhou University, Lanzhou, China, [4]Global Monitoring Laboratory, National Oceanic and Atmospheric Administration (NOAA), Boulder, CO, USA, [5]Cooperative Institute for Research in Environmental Sciences (CIRES), University of Colorado, Boulder, CO, USA, [6]Chemical Sciences Laboratory, National Oceanic and Atmospheric Administration (NOAA), Boulder, CO, USA, [7]Finnish Meteorological Institute (FMI), Helsinki, Finland, [8]Laboratoire de l'Atmosphère et des Cyclones (LACy, UMR 8105, CNRS, Météo-France Université de La Réunion), Saint-Denis, France, [9]National Institute of Water and Atmospheric Research (NIWA), Lauder, New Zealand, [10]Guangzhou Institute of Tropical and Marine Meteorology, Meteorological Administration, Guangzhou, China, [11]State Key Laboratory of Atmospheric Boundary Layer Physics and Atmospheric Chemistry, Institute of Atmospheric Physics, Chinese Academy of Sciences, Beijing, China, [12]Department of Atmospheric and Oceanic Sciences and Laboratory for Atmospheric and Space Physics, University of Colorado, Boulder, CO, USA

Abstract Approximately 150 Tg of water vapor and 0.42 Tg of sulfur dioxide were injected directly into the stratosphere by the January 2022 Hunga volcanic eruption, which represents the largest water vapor injection in the satellite era. A comparison of numerical simulations to balloon-borne and satellite observations of the water-rich plume suggests that particle coagulation contributed to the Hunga aerosol's effective dry radius increase from 0.2 μm in February to around 0.4 μm in March. Our model suggests that the stratospheric aerosol effective radius is persistently perturbed for years by moderate and large-magnitude volcanic events, whereas extreme wildfire events show limited impact on the stratospheric background particle size. Our analysis further suggests that both the particle optical efficiency and the aerosols' stratospheric lifetime explain Hunga's unusually large aerosol optical depth per unit of the SO_2 injection, as compared with the Pinatubo eruption.

Plain Language Summary The Hunga Tonga-Hunga Ha'apai (HTHH) submarine volcano erupted in January 2022, injecting a modest amount of SO_2 but a record amount of water vapor relative to other eruptions into the mid-stratosphere observed in the satellite era. Our climate model simulations of the stratospheric aerosol suggest that the large water vapor injection caused the new particle formation of many new sulfuric acid solution particles with small radius, enhancing the collision efficiency. Rapid collision led to a peak radius of 0.2 μm by February and 0.4 μm by March of 2022. Our analysis finds that both particle optical properties and aerosol persistence collectively exert an influence on normalized anomaly aerosol optical depth, explaining the high aerosol optical depth per unit emission of SO_2 by HTHH, relative to the 1991 Pinatubo eruption.

Key Points:

- Co-injected water vapor triggered a sudden and large production of aerosols, followed by a fast particle growth via coagulation
- Simulations and observations from La Réunion and Lauder suggest that the stratospheric aerosol size was elevated for 2 years
- Both the high optical efficiency and long stratospheric lifetime of HTHH aerosol contribute to a higher AOD per unit emission than Pinatubo

Supporting Information:

Supporting Information may be found in the online version of this article.

Correspondence to:

P. Yu,
pengfei.yu@colorado.edu

Citation:

Li, C., Peng, Y., Asher, E., Baron, A. A., Todt, M., Thornberry, T. D., et al. (2024). Microphysical simulation of the 2022 Hunga volcano eruption using a sectional aerosol model. *Geophysical Research Letters*, *51*, e2024GL108522. https://doi.org/10.1029/2024GL108522

Received 27 JAN 2024
Accepted 20 MAY 2024

Author Contributions:

Conceptualization: Pengfei Yu
Data curation: Elizabeth Asher, Alexandre A. Baron, Michael Todt, Troy D. Thornberry, Stephanie Evan, Jerome Brioude, Penny Smale, Richard Querel, Karen H. Rosenlof, Jingyuan Xu, Jianchun Bian
Formal analysis: Chenwei Li, Yifeng Peng, Luxi Zhou, Pengfei Yu
Funding acquisition: Pengfei Yu
Investigation: Chenwei Li, Yifeng Peng, Owen B. Toon, Yunqian Zhu
Methodology: Pengfei Yu
Project administration: Pengfei Yu
Supervision: Pengfei Yu

1. Introduction

The Hunga submarine volcano (20.54°S 175.38°W) erupted on January 13–15 of 2022. The Hunga eruption released moderate amounts of sulfur dioxide (SO_2) gas (0.4–0.5 Tg), as well as 150 Tg of water vapor directly into the stratosphere (Millan et al., 2022; Vömel et al., 2022; Xu et al., 2022). The injection heights span up to the mesopause (~50 km) with the bulk injected at around 25–30 km, higher than previous volcanic injection heights of the 20th–21st centuries (less than 20 km) (Baron et al., 2023; Carr et al., 2022; Proud et al., 2022; Taha et al., 2022; Yuen et al., 2022). Recent modeling studies have shown that this direct co-injection of water vapor and SO_2 led to sulfate aerosols with a surprisingly large particle size and long lifetime in the stratosphere, which is supported by both satellite and in situ observations (Asher et al., 2023; Khaykin et al., 2022; Tilmes et al., 2018; Yu et al., 2023; Zhu et al., 2022).

Aerosol microphysical properties are a major source of uncertainty in evaluating the stratospheric and climate effects from volcanic eruptions (Ansmann et al., 2022; Hamill et al., 1977; Kremser et al., 2016; Sekiya

Writing – original draft: Chenwei Li, Pengfei Yu
Writing – review & editing: Elizabeth Asher, Luxi Zhou, Kai Qie, Jianchun Bian, Owen B. Toon, Yunqian Zhu, Pengfei Yu

et al., 2016). Many previous studies have investigated the microphysical processes (e.g., nucleation, condensation/evaporation, and coagulation) of the stratospheric sulfate aerosol following volcanic eruptions (Dhomse et al., 2014; English et al., 2013; Wrana et al., 2023; Zhu et al., 2022). Zhu et al. (2022) showed that Hunga's water injection shortened the lifetime of SO_2 vapor, which accelerated nucleation of sulfuric acid particles leading to coagulation and producing a large particle effective radius in the volcanic plume. However, the extent to which the injected water vapor affects the coagulation of Hunga's particles and the long-term size evolution of stratospheric background particles remains unclear. The Hunga plume exhibited large particles, requiring comparison with moderate and large magnitude volcanic eruptions, as well as extreme wildfire events.

Stratospheric volcanic aerosols increase the stratospheric aerosol optical depth (sAOD) and influence the Earth's radiative balance. A four-fold to five-fold increase in the sAOD was observed after the Hunga eruption, producing an optical depth that exceeded by far that of any other volcanic or wildfire event in the last three decades (Khaykin et al., 2022; Schoeberl et al., 2022, 2023; Yu et al., 2023; Zhu et al., 2022). Compared with Mt. Pinatubo eruption in 1991, a large magnitude eruption, HTHH generates a high sAOD per unit of injected SO_2 mass (Asher et al., 2023). Asher et al. (2023) suggested that the ∼560 nm diameter mode of aerosol particles inside of the volcanic plume led to the high sAOD relative to its emission.

Here, we compare simulations from a sectional aerosol-climate model (CESM1-CARMA) (Yu et al., 2015) with satellite and balloon-borne observations to investigate the microphysical processes that contributed to the evolution of the stratospheric aerosol effective radius following the Hunga eruption. We also quantitively evaluate the factors contributing to the high AOD of Hunga relative to its modest size of the injection.

2. Methods

2.1. CESM1-CARMA Aerosol Model

We simulated the microphysical processes of the Hunga eruption using a sectional aerosol microphysics model, the Community Aerosol and Radiation Model for Atmospheres (CARMA), coupled with the specified dynamics (SD) version of the Community Earth System Model Version 1 (CESM1-CARMA) (Bardeen et al., 2008; Toon et al., 1988; Yu et al., 2015). Simulations are nudged to Modern-Era Retrospective analysis for Research and Applications meteorology (Rienecker et al., 2011). The model was run on a grid of 1.9° latitude × 2.5° longitude with 56 vertical layers from the surface up to 45 km. The modeled winds and temperatures were nudged to the Goddard Earth Observing System 5 (GEOS-5) reanalysis data set (Molod et al., 2015). In our simulations, CARMA is fully coupled to the chemistry and radiation scheme of CESM. The gas-phase chemical scheme used is the Model for Ozone and Related Chemical Tracers (MOZART) that is used for both tropospheric (Emmons et al., 2010) and stratospheric chemistry (English et al., 2011; Mills et al., 2016). Unlike the modal aerosol model used by Zhu et al. (2022), the CESM1-CARMA aerosol model is a sectional model that tracks two groups of aerosols in 20 discrete size bins each: the first group is composed of pure sulfate and the other is composed of internal mixtures of various aerosol components including sulfate (in the form of sulfuric acid), organics, black carbon, dust, and salt. The dry radius of the pure sulfate particles ranges from 0.2 nm to 1.3 μm, and the dry radius of the mixed particles ranges from 0.05 to 8.7 μm (Yu et al., 2015). For both groups, the wet (ambient) radius is determined by the modeled relative humidity. For the pure sulfate group, a parameterization by (Tabazadeh et al., 1997) determines the weight percent of H_2SO_4 in the H_2SO_4/H_2O particles while in the mixed group, the wet radius is parameterized based on the weighted hygroscopicity of the internally mixed species (Petters & Kreidenweis, 2007).

Three sets of Hunga simulations were performed, initialized from January of 2022 to ending December of 2023. One set of simulations (named "Full-HTHH") considered 0.42 Tg SO_2 and 150 Tg water vapor injected between 25 and 30 km between 22°S and 14°S following Zhu et al. (2022). Note that we injected SO_2 with the same vertical distribution to that of water vapor. However, SO_2 was injected at lower altitudes than water vapor in Zhu et al. (2022). To identify the impact of injected water vapor from the Hunga eruption, another set of simulations (named "SO_2-only-HTHH") considered injections of SO_2 but not water vapor; the third set of simulations (named "Control") represented the unperturbed atmosphere without eruption. In addition, we compared the simulated microphysical processes among various volcanic and wildfire events. We performed simulations of the 1991 Mt. Pinatubo eruption, with 12 Tg SO_2 injected at 18–20 km between 0 and 15 ºN (Mills et al., 2016), and the Australian New Year (ANY) wildfire pyroCb event, with 0.9 Tg of smoke particles injected at 13 km (Yu et al., 2021). Note that the observed SO_2 injection by Pinatubo was 18 ± 4 Tg from most analyses (Carn

et al., 2016). The Mills et al. (2016) estimate may have been affected by using a modal aerosol model. However, the magnitude of the injection does not impact the results presented here all of which use the same sectional aerosol microphysics model.

2.2. Observed Water Vapor and Volcanic Aerosol

The Portable Optical Particle Spectrometer (POPS) is a light-weight balloon-borne instrument that measures particle number concentration and size within a 70 nm–1.25 μm radius range (Gao et al., 2016; Todt et al., 2023). Balloon-borne POPS measurements of the Hunga plumes at La Réunion island (21°S, 55°E) (Asher et al., 2023) and Lauder (45°S, 170°E) taken from January 2022 to September 2023 were used in our study. In addition, water vapor measured by the balloon-borne Cryogenic Frost-point Hygrometer (CFH) launched at Lijiang (100.22°E, 26.85°N) on 9 April 2022 was also used (Xu et al., 2022).

The simulated global distributions of stratospheric water vapor and aerosol optical depth were compared against satellite observations from the Microwave Limb Sounder (MLS) (Lambert et al., 2015) and the Stratospheric Aerosol and Gas Experiment on board the international space station (SAGE III/ISS) (Cisewski et al., 2014).

3. Results

3.1. Stratospheric Water and Aerosol Abundance

The simulated time series of the stratospheric water vapor anomalies (Figure S1a in Supporting Information S1) and the sAOD (Figure S1b in Supporting Information S1) were compared with MLS (Lambert et al., 2015) and SAGE III/ISS (Cisewski et al., 2014), respectively. Figure S1a in Supporting Information S1 shows that approximately 75% of the simulated global water vapor anomalies from Hunga were located in the upper stratosphere (1 to 30 hPa) in the first year since eruption. The model underestimates the observed water vapor in the upper stratosphere by ∼20 Tg. Both MLS data and the model suggest that Hunga water vapor in the upper stratosphere declined by ∼50% in the second year.

Figure S1b in Supporting Information S1 shows that the majority of aerosols stayed in the lower latitudes of the Southern Hemisphere (SH) in the first 3 months and were gradually transported toward the South Pole. Both the model and SAGE III/ISS observations show that the volcanic plume was transported to midlatitudes centered at 45°S by mid-April (3.5 months after the eruption) and stayed out of the polar vortex due to the transport barrier in the first year (high sAOD is not observed poleward of 60 S). After the polar vortex broke down in December of 2022, some Hunga plumes were transported into the polar region (60°S–90 S) with sAOD elevated by 0.003. A small amount of Hunga plumes were transported to the Northern Hemisphere (NH) as observed in Xu et al. (2022). In the second year, the simulated Hunga AOD anomalies were homogeneously distributed in SH, with a hemispheric average of about 0.015, which is 42.86% of the stratospheric background sAOD. Note that a small amount of the simulated Hunga water vapor was transported to the NH starting from November of 2022. Figure S1c in Supporting Information S1 shows that the simulated stratospheric sAOD anomalies agreed consistently with the observations to within 7% with a correlation coefficient of 0.892.

3.2. Vertical Distributions of the Hunga Particle Size Distributions

Figure 1a compares the simulated and observed vertical distributions of the aerosol effective radius for the particle size range from 70 nm to 1.25 μm in diameter. Balloon-borne particle size distributions were measured at La Réunion Island (21°S, 55°E) from January to March of 2022 using POPS (Asher et al., 2023). In general, the model reproduces the observed aerosol effective radius both in the troposphere and perturbed stratosphere. The observed and simulated effective radius of aerosols in the troposphere between 10 and 15 km was approximately 100–150 nm, the lowest size the POPS can measure. The effective radius increases to about 200 nm with altitudes from 17.5 to 20 km. The elevated effective particle radius in the stratosphere is consistent with the in situ airborne aerosol measurements in mid-latitudes of the upper troposphere and lower stratosphere (UTLS) by Murphy et al. (2021). On 22 January 2022, the peak aerosol effective radius inside of the Hunga volcanic plume was approximately 300 nm near 26–27.5 km. Larger peaks over 400 nm were measured by two balloon launches in February–March of 2022 at lower altitudes between 23 and 25 km. Both model and observations suggested that the stratospheric aerosol effective radius is elevated from 200 nm to about 400 nm in the first few months due to 2022 Hunga eruption. The evolution and the microphysical processes associated with the particles size changes

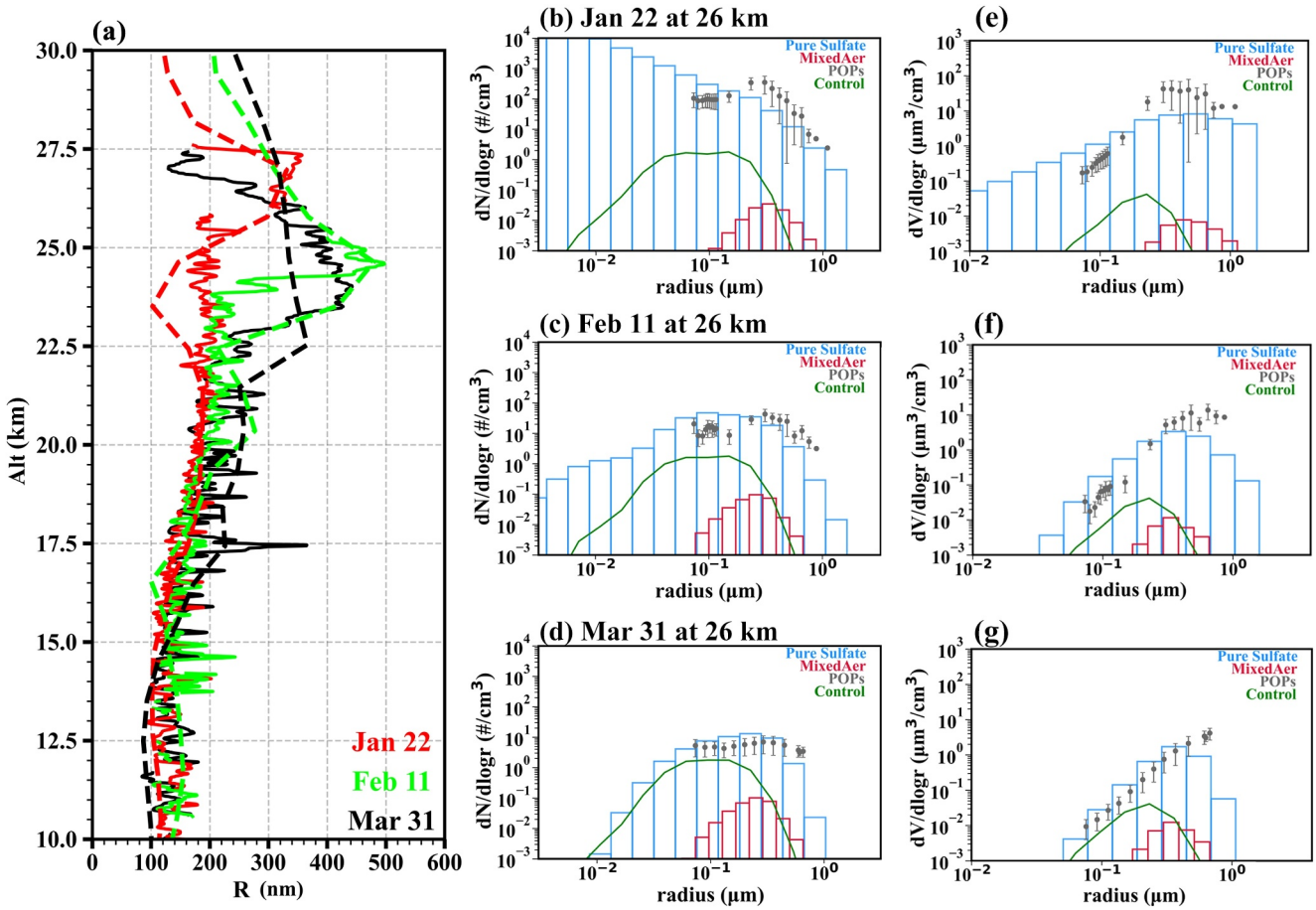

Figure 1. Comparison of the aerosol size with balloon-borne observations. (a) Observations of the aerosol effective radius (unit: nm) inside of the volcanic plume from the portable optical particle spectrometers (POPS) launched in Réunion Island (21°S, 55.4°E) on January 22, February 11 and March 31 of 2022 are denoted by solid lines. Simulated daily mean vertical distributions of aerosol effective radius inside the plume located near Réunion Island on the three balloon launch days are denoted by the dashed lines. (b–d) Comparison of the simulated aerosol number size distributions (dN/dlogr, unit: #/cm^3) with balloon observations (denoted by the black filled circles) at 26 km (Asher et al., 2023) on the three balloon launch days shown in each panel, respectively. Simulated aerosol number size distributions for the pure sulfate and mixed aerosols (detailed model settings in Section 2 and Yu et al., 2015) are denoted by the blue and red boxes, respectively. The simulated pure sulfate number size distributions on each balloon launch day without HTHH eruption are denoted by the green solid lines in each panel, respectively. Panels (e–g) same as panels (b–d) but for volume distribution (dV/dlogr, unit: μm^3/cm^3).

are discussed in Section 3.3. Shown in Figure S2 in Supporting Information S1, without water vapor injection, the model underestimates the observed number concentration for particles greater than 0.2 μm in diameter. The comparison between the simulated size distributions with water vapor injection (Figure 2) and without water vapor injection (Figure S2 in Supporting Information S1) indicates that water vapor accelerates the coagulation growth of the Hunga particles indirectly by accelerating the oxidation rate of SO_2, which increases the concentration of small aerosols.

The measured and simulated number and volume size distributions inside of the plume during the three balloon launches are shown in Figures 1b–1g. Measured size distributions range from 140 nm to 3 μm, while the simulated aerosol size distribution span across four orders of magnitude, allowing for diagnostics of the early evolution of the volcanic plumes. As expected, the modeled stratospheric size distributions were dominated by the pure sulfuric acid following Hunga eruption. In January, the simulated particle number concentrations around 10 nm in diameter were elevated by seven orders of magnitude compared with the control simulation due to efficient nucleation of sulfate in the first few weeks. The simulated nucleation mode particle number concentrations around 10 nm were still elevated by two orders of magnitude in February (Figure 1c), however no enhancement in the nucleation mode was simulated on 31 March 2022 (Figure 1d).

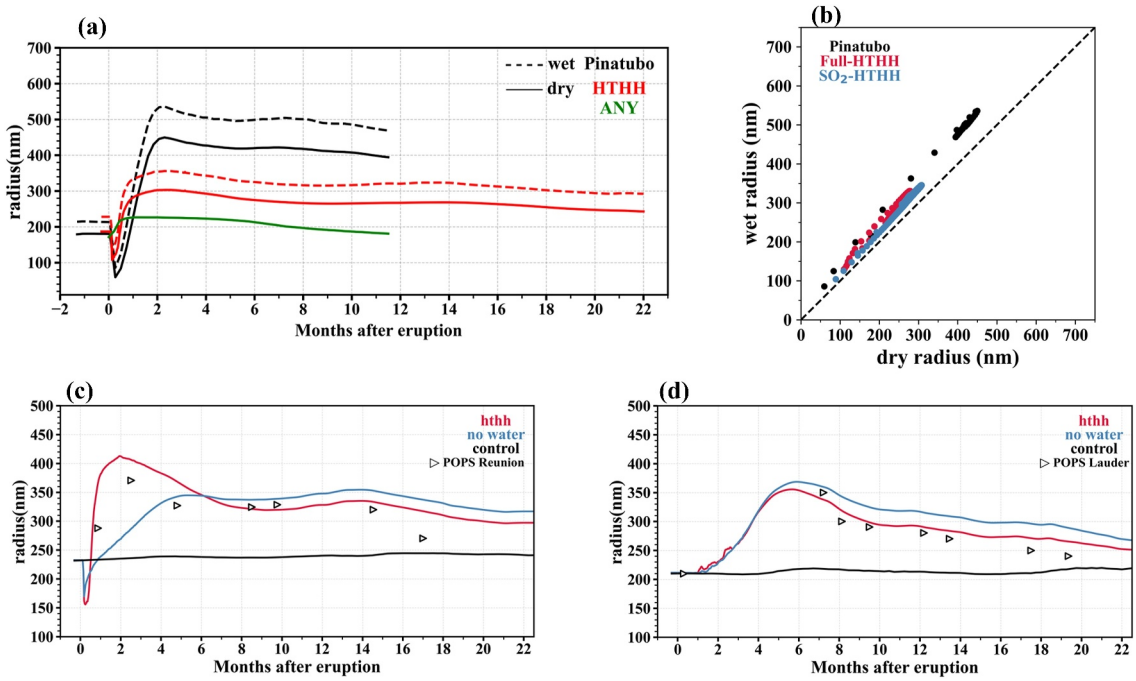

Figure 2. (a) Simulated temporal evolution of the aerosol effective dry and wet radius (unit: nm) averaged over 60°S–60°N and between 22 and 28 km after HTHH eruption is denoted by the solid and dashed red line, respectively. The simulated particle effective dry and wet radius averaged over 60°S–60°N and between 18 and 20 km after the 1991 Pinatubo event and the 2019–2020 ANY wildfire event are shown in black and green lines, respectively. (b) Scatterplot comparing the simulated dry and wet effective radius averaged over 60°S–60°N for the Pinatubo, Full-HTHH and the SO_2-only-HTHH simulations denoted by the black, red and blue dots, respectively. The black dashed lines denote 1:1 relationship between the simulated dry and wet effective radius. (c, d) Simulated temporal evolution of the aerosol effective wet radius averaged over 30°S–0°S and between 20 and 25 km. The simulated aerosol effective radius in the Full- HTHH and SO_2-only-HTHH scenarios are denoted by the blue and red solid lines, respectively. The black line denotes the simulated stratospheric background aerosol effective wet radius in the control simulation without the influence of HTHH. Observation from portable optical particle spectrometers (POPS) launched in Réunion Island (21°S, 55.4°E) and Lauder (45°S, 170°E) are denoted by the open triangles.

3.3. Evolution of Hunga Aerosol Effective Radius

As shown in Figure 2a, the simulated evolution of the near-global (60°S-60°N) mean aerosol effective radius between 22 and 28 km after the Hunga eruption exhibited three stages: (a) a reduction in the effective dry radius from the unperturbed background value of ∼180 nm to around 100 nm due to the enormous amount of new particles formed due to the oxidation and nucleation processes in weeks one and two; (b) the simulated effective dry radius peaked at ∼280 nm via effective coagulation inside of the plume when the particle number concentration was high in weeks 3 and 4; (c) the slow decline in the effective dry radius, as the larger particles preferentially sedimented out of the stratosphere after the first month. The simulated near global stratospheric aerosol effective dry radius remained elevated (∼240 nm) compared with the background value (∼180 nm) for 2 years after the eruption. Three similar stages of effective radius were found for the 1991 Pinatubo Eruption, a large-magnitude eruption (Figure 2a). The large-magnitude injection of SO_2 from 1991 Pinatubo eruption resulted more new particle formation and a lower effective dry radius (∼60 nm) in the first stage, which accelerated the coagulation efficiency and led to the formation of aerosols with larger particle peak effective dry radius at 450 nm within 2 months. Note that in our model simulations, we inject SO_2 at 18–20 km following Mills et al. (2016). However, Quaglia et al. (2023) showed that the injection altitudes of Pinatubo ranged from 18 to 30 km. Additionally, multiple climate models have demonstrated large variability in the simulated effective dry radius with various injection altitudes. Consequently, the evolution of the dry effective radius is expected to be dependent on the injection altitude range utilized in model simulations. After extreme wildfire events, which inject large amounts of organic particles into the stratosphere (e.g., 2019–2020 Australian New-year, ANY event), the aerosol effective radius increases slightly in the initial stage and slowly declines with time. Note that we assumed that the primary aerosol emissions dominate the ANY event, and we ignored the secondary formation of organics in the fire plume in our model simulation. Besides, following previous modeling study on ANY event (Yu et al., 2021), we ignored the detailed chemical processes near the fire source but directly injected smoke

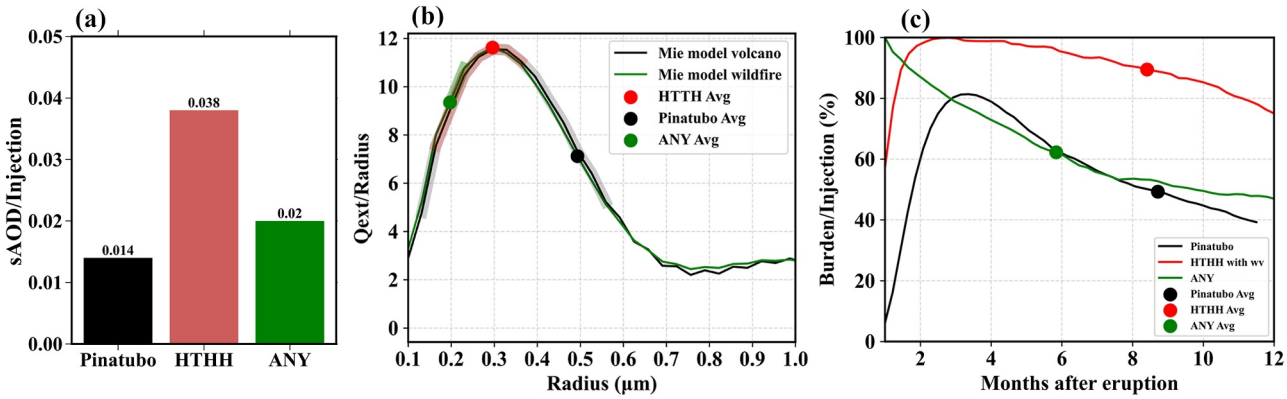

Figure 3. (a) Calculated stratospheric between 60°S and 60°N stratospheric aerosol optical depth (sAOD) per injection (sAOD/Injection) for HTHH, Pinatubo and ANY are denoted in red, black and green bars respectively. (b) The volcanic and wildfire aerosol extinction efficiency normalized by the size of the particle (Qext/Radius) based on the Mie theory are denoted in black and green solid lines, respectively. The calculated global mean effective radius above 200 mb for HTHH, Pinatubo and ANY averaged in the first year since eruption are denoted in red, black and green circles, respectively. The simulated range of the stratospheric effective radius following the three events are denoted in red, black and green shaded region, respectively. (c) Simulated temporal evolution of the global mean aerosol burden anomalies above 200 mb normalized by the stratospheric injection (Burden/Injection) for Pinatubo, HTHH and ANY events are denoted in black, red and green solid lines, respectively. The stratospheric aerosol burden normalized by the injection for the three events averaged in the first year are denoted by the filled and color-coded circles, respectively.

aerosol at ~12 km, with the majority of the aerosol mass concentrated in the accumulation mode, based on the optical measurements near the fire source (Yu et al., 2015). Figure S3 in Supporting Information S1 shows the simulated smoke particles from the ANY event were mainly in the accumulation mode with comparatively lower particle number concentrations and a lower coagulation rate compared with newly nucleated particles formed after volcanic eruption. Lower particle number concentrations from the ANY event led to smaller coagulation rates. Consequently, there is a limited change in the stratospheric aerosol effective radius in the first 3 weeks after the ANY event.

Hydroscopic growth of aerosols is mostly determined by the ambient relative humidity and aerosol hygroscopicity. Figure 2a shows that the simulated wet (ambient) effective radius follows the evolution of the dry radius in all three stages discussed above. The simulated evolution of the wet (ambient) effective radius was primarily driven by the dry radius. However, the hydroscopic growth of particles from the Pinatubo volcanic eruption was slightly higher than that from Hunga eruption as shown in Figure 2b. This greater hydroscopic growth when the plume is spread out after a few months since eruption is because the Pinatubo injection was at lower altitudes (i.e., 18–20 km (Mills et al., 2016)), with higher relative humidity than the altitudes of Hunga particles (i.e., 22–28 km).

Zhu et al. (2022) showed that the water vapor injection from Hunga likely accelerated the oxidation of SO_2 and promoted rapid formation of the sulfate aerosol compared with a case if only SO_2 (and no water vapor) was injected. Consistent with this study, our Hunga simulation showed low effective radius in the first stage compared to the simulation without a water vapor injection (Figure 2c). Shown in Zhu et al. (2020), simulated evolution of the aerosol size distribution following Mt. Kelut volcano is dominated by the coagulation process. Because more particles formed in the first stage with the water injection due to faster oxidation of SO_2, the coagulation of particles was much faster with the addition of stratospheric water vapor. The simulated effective dry radius also reached the peak in 1 month as a result of the water vapor injection, while it took 4 months to reach its peak without water vapor injection. Simulations and observations from La Réunion and Lauder suggest that the stratospheric aerosol effective size was persistently elevated for 2 years (Figures 2c and 2d).

4. Discussions

The Hunga eruption resulted in a four-fold to five-fold increase in the global mean sAOD, exceeding the optical depth of any volcanic or wildfire event in the last three decades by far (Khaykin et al., 2022). Asher et al. (2023) suggested that the large size of the Hunga particles with a mode radius of ~280 nm was responsible for the observed high extinction coefficients in the volcanic plume. We used CARMA to quantify the factors contributing to the large global mean sAOD of Hunga for a relatively low SO_2 injection. As shown in Figure 3a, the simulated

global and annual mean normalized sAOD (defined by the sAOD divided by the injection) of Hunga is 2.7-fold larger than Pinatubo's and 1.9-fold larger than ANY's.

To understand why the Hunga global mean sAOD is so large, first we assume that the aerosol column mass and the optical depth are uniform over an area of the Earth (A). Next, we separate the global mean sAOD per mass injected (E) into two terms in Equation 1: one term is sAOD per aerosol stratospheric mass burden (B); the other term is stratospheric mass burden per mass injected. Both terms vary over time. The first term varies due to the change in radius with time, the second varies due to sedimentation (removal of mass from the stratosphere).

$$\frac{sAOD}{E} = \frac{sAOD}{B} * \frac{B}{E} \tag{1}$$

According to Mie Scattering Theory and Clyne et al. (2021), we know that for a homogeneous layer of thickness Δz

$$sAOD = Q_{ext} \pi r^2 \cdot N \cdot \Delta z \tag{2}$$

Q_{ext} denotes the particle optical extinction efficiency, r denotes the particle radius and N is the number concentration. Replacing N with column mass density ($M = B/A$) Equation 2 is transformed to

$$\frac{sAOD}{B} = \frac{3}{4\rho A} * \frac{Q_{ext}}{r} \tag{3}$$

where ρ denotes the particle density.

Based on Equation 3, we know that the global mean sAOD for fixed global mass burden, ($\frac{sAOD}{B}$), is proportional to $\frac{Q_{ext}}{r}$. Figure 3b shows the relation between the size of particle (r) and the optical efficiency ($\frac{Q_{ext}}{r}$) (i.e., AOD per fixed mass burden) based on the Mie theory (Clyne et al., 2021). Figure 3b shows that particles with the radius around 0.3 μm have the largest optical efficiency ($\frac{Q_{ext}}{r}$) with similar finding reported in Clyne et al. (2021). Note that in the model, the refractive indices of BC are set at 1.95–0.79i at mid-visible light, while the refractive indices of OC and sulfate are set at 1.43–0i. Because the wildfire smoke aerosol is dominated by OC, with mass fraction of about 98% (Yu et al., 2019), the total extinction efficiencies (Q_{ext}) of wildfire smoke and volcanic aerosol are similar. Figure 2a shows the simulated effective radius in the first year after the Hunga eruption was about 0.28 μm, which is near the peak of the theoretical aerosol extinction efficiency shown in Figure 3b. Figure 2a shows the simulated effective radius was over 0.4 μm for most of the year after the Pinatubo eruption. Additionally, the ANY event exhibited a smaller effective radius around 0.2 μm. Our model suggests that the global and annual mean sAOD per fixed mass burden ($\frac{Q_{ext}}{r}$) of the Hunga was 1.5-fold higher than that of the Pinatubo event and 1.25-fold higher than that of the ANY wildfire. However, the optical efficiency alone does not explain why the simulated global and annual mean normalized sAOD (sAOD/E) of Hunga was 2.7-fold larger than Pinatubo's and 1.9-fold larger than ANY's sAOD (Figure 3a).

The fraction of mass remaining, ($\frac{B}{E}$), is highly sensitive to the altitude and latitudes of injection. The value of the annual mean $\frac{B}{E}$ is proportional to aerosol' lifetime. As shown in Figure 3c, the modeled $\frac{B}{E}$ of Hunga remains about 1.8-fold larger than that of Pinatubo and also 1.45-fold higher than that of the ANY wildfire averaged over the first year after the injection. The long lifetime of Hunga particles is largely caused by its extremely high injection altitude (i.e., 25–30 km). Based on our simple analysis, the 2019–2020 ANY fire shows 20% smaller optical efficiency ($\frac{Q_{ext}}{r}$) and a 30% smaller fraction of mass remaining ($\frac{B}{E}$) in the first year when compared with Hunga. In contrast, the 1991 Pinatubo eruption shows 40% smaller optical efficiency ($\frac{Q_{ext}}{r}$) and 60% smaller fraction of mass remaining ($\frac{B}{E}$) than that of Hunga. Our study suggests that both high optical efficiency and long aerosol lifetime contribute to a higher sAOD relative to its emission of Hunga.

5. Summary

We simulated the microphysical processes affecting stratospheric aerosols from the Hunga eruption using a sectional aerosol model coupled with a climate model, CESM1-CARMA. Simulated stratospheric aerosol and

water vapor anomalies were compared against observations from MLS, SAGE III/ISS and in situ balloon-borne POPS launched in La Réunion Island (21°S, 55.4°E) and Lauder (45°S, 170°E). Both the model and satellite measurements suggested that the volcanic plume remained in the lower latitudes of the Southern Hemisphere in the first 3 months and was excluded from the polar vortex due to the transport barrier in the austral summer/spring of 2022. Comparisons of the simulated aerosol size distributions with balloon-borne observations showed that the peak effective radius (~0.4 μm) occurred at 20–25 km altitude in March 2022, which is significantly greater than the background aerosol effective radius (~0.2 μm or smaller).

We also compared the simulated temporal distributions of the particle effective radius of the Hunga aerosol layer with those of other volcanic and wildfire events. The injection of water vapor accelerated the oxidation of SO_2 as explained in Zhu et al. (2022). The comparison suggested the injected water vapor from Hunga led to the rapid formation of new particles by increasing the SO_2 oxidation rate, enhancing coagulation efficiency resulting in the aerosol particles reaching peak wet radius (~350 nm) more rapidly than in the case of Pinatubo. Our study indicates that the stratospheric aerosol effective radius is perturbed by moderate and large-magnitude volcanic events for years after the injection. Note that we ignored the detailed chemical processes near the fire source, but injected the aerosols in the upper troposphere directly and in the accumulation mode bins. The simulated effective radius from extreme wildfire events is fixed at the time of injection.

Our study also reveals that both the optical efficiency and aerosol lifetime contributed to the observed higher stratospheric sAOD normalized by emission of Hunga, when compared with the Pinatubo volcanic eruption and the ANY wildfire event. The high optical efficiency of the Hunga particles due to their optimal particle size accounted for 1.5-fold higher normalized AOD observed in Hunga compared to Pinatubo. In addition to the optical efficiency, Hunga's high injection height significantly extended the lifetime of particles and consequently elevated the aerosol burden in the stratosphere. The simulated high fraction of mass remaining of Hunga's aerosols accounted for another 1.8-fold higher normalized AOD than Pinatubo.

Data Availability Statement

MLS data (Lambert et al., 2015) can be obtained from https://acdisc.gesdisc.eosdis.nasa.gov/data//Aura_MLS_Level2/ML2H2O.004/2022/ and SAGE III/ISS data (NASA/LARC/SD/ASDC, 2017 can be obtained from https://doi.org/10.5067/ISS/SAGEIII/SOLAR_BINARY_L2-V5.2). Simulation data used in this work are available in Li and Yu (2024). The data analysis provided in this paper was created by NCL (The NCAR Command Language, 2019). All Figures were made with Matplotlib version 3.8.2 (The Matplotlib Development Team, 2023).

Acknowledgments
This work is supported by the second Tibetan Plateau Scientific Expedition and Research Program (STEP, 2019QZKK0604) and the National Natural Science Foundation of China (42121004, 42175089). Chenwei Li is supported by Guangzhou Science and Information Bureau project (2024A04J0742). Luxi Zhou is supported by the National Natural Science Foundation of China (42205117). The CESM project is supported by the National Science Foundation and the Office of Science (BER) of the U.S. Department of Energy. We acknowledge high-performance computing support from Cheyenne (https://doi.org/10.5065/D6RX99HX) provided by NCAR's Computational and Information Systems Laboratory, sponsored by the National Science Foundation.

References

Ansmann, A., Ohneiser, K., Chudnovsky, A., Knopf, D. A., Eloranta, E. W., Villanueva, D., et al. (2022). Ozone depletion in the Arctic and Antarctic stratosphere induced by wildfire smoke. *Atmospheric Chemistry and Physics*, *22*(17), 11701–11726. https://doi.org/10.5194/acp-22-11701-2022

Asher, E., Todt, M., Rosenlof, K., Thornberry, T., Gao, R. S., Taha, G., et al. (2023). Unexpectedly rapid aerosol formation in the Hunga Tonga plume. *Proceedings of the National Academy of Sciences of the U S A*, *120*(46), e2219547120. https://doi.org/10.1073/pnas.2219547120

Bardeen, C. G., Toon, O. B., Jensen, E. J., Marsh, D. R., & Harvey, V. L. (2008). Numerical simulations of the three-dimensional distribution of meteoric dust in the mesosphere and upper stratosphere. *Journal of Geophysical Research*, *113*(D17), D17202. https://doi.org/10.1029/2007JD009515

Baron, A., Chazette, P., Khaykin, S., Payen, G., Marquestaut, N., Bègue, N., & Duflot, V. (2023). Early evolution of the stratospheric aerosol plume following the 2022 Hunga Tonga-Hunga Ha'apai eruption: Lidar observations from reunion (21°S, 55°E). *Geophysical Research Letters*, *50*(10), e2022GL101751. https://doi.org/10.1029/2022GL101751

Carn, S. A., Clarisse, L., & Prata, A. J. (2016). Multi-decadal satellite measurements of global volcanic degassing. *Journal of Volcanology and Geothermal Research*, *311*, 99–134. https://doi.org/10.1016/j.jvolgeores.2016.01.002

Carr, J. L., Horváth, Á., Wu, D. L., & Friberg, M. D. (2022). Stereo plume height and motion retrievals for the record-setting Hunga Tonga-Hunga Ha'apai eruption of 15 January 2022. *Geophysical Research Letters*, *49*(9), e2022GL098131. https://doi.org/10.1029/2022GL098131

Cisewski, M. S., Zawodny, J. M., Gasbarre, J. F., Eckman, R. S., Topiwala, N., Rodriguez-Alvarez, O., et al. (2014). The Stratospheric Aerosol and Gas Experiment (SAGE III) on the International Space Station (ISS) Mission. In *Paper presented at the SPIE remote sensing. Proc. SPIE 9241, sensors, Systems, and next-generation satellites XVIII*. 924107. https://doi.org/10.1117/12.2073131

Clyne, M., Lamarque, J. F., Mills, M. J., Khodri, M., Ball, W., Bekki, S., et al. (2021). Model physics and chemistry causing intermodel disagreement within the VolMIP-Tambora Interactive Stratospheric Aerosol ensemble. *Atmospheric Chemistry and Physics*, *21*(5), 3317–3343. https://doi.org/10.5194/acp-21-3317-2021

Dhomse, S. S., Emmerson, K. M., Mann, G. W., Bellouin, N., Carslaw, K. S., Chipperfield, M. P., et al. (2014). Aerosol microphysics simulations of the Mt.~Pinatubo eruption with the UM-UKCA composition-climate model. *Atmospheric Chemistry and Physics*, *14*(20), 11221–11246. https://doi.org/10.5194/acp-14-11221-2014

Emmons, L. K., Walters, S., Hess, P. G., Lamarque, J.-F., Pfister, G. G., Fillmore, D., et al. (2010). Description and evaluation of the model for ozone and related chemical tracers, version 4 (MOZART-4). *Geoscientific Model Development*, *3*(1), 43–67. https://doi.org/10.5194/gmd-3-43-2010

English, J. M., Toon, O. B., & Mills, M. J. (2013). Microphysical simulations of large volcanic eruptions: Pinatubo and Toba. *Journal of Geophysical Research: Atmospheres*, *118*(4), 1880–1895. https://doi.org/10.1002/jgrd.50196

English, J. M., Toon, O. B., Mills, M. J., & Yu, F. (2011). Microphysical simulations of new particle formation in the upper troposphere and lower stratosphere. *Atmospheric Chemistry and Physics*, *11*(17), 9303–9322. https://doi.org/10.5194/acp-11-9303-2011

Gao, R. S., Telg, H., McLaughlin, R. J., Ciciora, S. J., Watts, L. A., Richardson, M. S., et al. (2016). A light-weight, high-sensitivity particle spectrometer for PM2.5 aerosol measurements. *Aerosol Science and Technology*, *50*(1), 88–99. https://doi.org/10.1080/02786826.2015.1131809

Hamill, P., Toon, O. B., & Kiang, C. S. (1977). Microphysical processes affecting stratospheric aerosol particles. *Journal of the Atmospheric Sciences*, *34*(7), 1104–1119. https://doi.org/10.1175/1520-0469(1977)034<1104:MPASAP>2.0.CO;2

Khaykin, S., Podglajen, A., Ploeger, F., Grooß, J.-U., Tence, F., Bekki, S., et al. (2022). Global perturbation of stratospheric water and aerosol burden by Hunga eruption. *Communications Earth & Environment*, *3*(1), 316. https://doi.org/10.1038/s43247-022-00652-x

Kremser, S., Thomason, L. W., von Hobe, M., Hermann, M., Deshler, T., Timmreck, C., et al. (2016). Stratospheric aerosol—Observations, processes, and impact on climate. *Reviews of Geophysics*, *54*(2), 278–335. https://doi.org/10.1002/2015RG000511

Lambert, A., Read, W., & Livesey, N. (2015). MLS/Aura level 2 water vapor (H_2O) mixing ratio V004, Greenbelt, MD, USA, Goddard Earth Sciences Data and Information Services Center (GES DISC). [Dataset]. https://doi.org/10.5067/Aura/MLS/DATA2009

Li, C., & Yu, P. (2024). Data from: Microphysical simulation of the 2022 Hunga Volcano Eruption using a sectional aerosol model. *Zenodo*. https://doi.org/10.5281/zenodo.11047946

Millan, L., Santee, M. L., Lambert, A., Livesey, N. J., Werner, F., Schwartz, M. J., et al. (2022). The Hunga Tonga-Hunga Ha'apai hydration of the stratosphere. *Geophysical Research Letters*, *49*(13), e2022GL099381. https://doi.org/10.1029/2022gl099381

Mills, M. J., Schmidt, A., Easter, R., Solomon, S., Kinnison, D. E., Ghan, S. J., et al. (2016). Global volcanic aerosol properties derived from emissions, 1990–2014, using CESM1(WACCM). *Journal of Geophysical Research: Atmospheres*, *121*(5), 2332–2348. https://doi.org/10.1002/2015JD024290

Molod, A., Takacs, L., Suarez, M., & Bacmeister, J. (2015). Development of the GEOS-5 atmospheric general circulation model: Evolution from MERRA to MERRA2. *Geoscientific Model Development*, *8*(5), 1339–1356. https://doi.org/10.5194/gmd-8-1339-2015

Murphy, D. M., Froyd, K. D., Bourgeois, I., Brock, C. A., Kupc, A., Peischl, J., et al. (2021). Radiative and chemical implications of the size and composition of aerosol particles in the existing or modified global stratosphere. *Atmospheric Chemistry and Physics*, *21*(11), 8915–8932. https://doi.org/10.5194/acp-21-8915-2021

NASA/LARC/SD/ASDC. (2017). SAGE III/ISS L2 solar event species profiles (Native) V052 [Dataset]. *NASA Langley Atmospheric Science Data Center DAAC*. https://doi.org/10.5067/ISS/SAGEIII/SOLAR_BINARY_L2-V5.2

Petters, M. D., & Kreidenweis, S. M. (2007). A single parameter representation of hygroscopic growth and cloud condensation nucleus activity. *Atmospheric Chemistry and Physics*, *7*(8), 1961–1971. https://doi.org/10.5194/acp-7-1961-2007

Proud, S. R., Prata, A. T., & Schmauß, S. (2022). The January 2022 eruption of Hunga Tonga-Hunga Ha'apai volcano reached the mesosphere. *Science*, *378*(6619), 554–557. https://doi.org/10.1126/science.abo4076

Quaglia, I., Timmreck, C., Niemeier, U., Visioni, D., Pitari, G., Brodowsky, C., et al. (2023). Interactive stratospheric aerosol models' response to different amounts and altitudes of SO_2 injection during the 1991 Pinatubo eruption. *Atmospheric Chemistry and Physics*, *23*(2), 921–948. https://doi.org/10.5194/acp-23-921-2023

Rienecker, M. M., Suarez, M. J., Gelaro, R., Todling, R., Bacmeister, J., Liu, E., et al. (2011). MERRA: NASA's Modern-Era Retrospective analysis for research and applications. *Journal of Climate*, *24*(14), 3624–3648. https://doi.org/10.1175/JCLI-D-11-00015.1

Schoeberl, M. R., Wang, Y., Ueyama, R., Taha, G., Jensen, E., & Yu, W. (2022). Analysis and impact of the Hunga Tonga-Hunga Ha'apai stratospheric water vapor plume. *Geophysical Research Letters*, *49*(20), e2022GL100248. https://doi.org/10.1029/2022GL100248

Schoeberl, M. R., Wang, Y., Ueyama, R., Taha, G., & Yu, W. (2023). The cross equatorial transport of the Hunga Tonga-Hunga Ha'apai eruption plume. *Geophysical Research Letters*, *50*(4), e2022GL102443. https://doi.org/10.1029/2022GL102443

Sekiya, T., Sudo, K., & Nagai, T. (2016). Evolution of stratospheric sulfate aerosol from the 1991 Pinatubo eruption: Roles of aerosol microphysical processes. *Journal of Geophysical Research*, *121*(6), 2911–2938. https://doi.org/10.1002/2015JD024313

Tabazadeh, A., Toon, O. B., & Jensen, E. J. (1997). Formation and implications of ice particle nucleation in the stratosphere. *Geophysical Research Letters*, *24*(16), 2007–2010. https://doi.org/10.1029/97GL01883

Taha, G., Loughman, R., Colarco, P. R., Zhu, T., Thomason, L. W., & Jaross, G. (2022). Tracking the 2022 Hunga Tonga-Hunga Ha'apai aerosol cloud in the upper and middle stratosphere using space-based observations. *Geophysical Research Letters*, *49*(19), e2022GL100091. https://doi.org/10.1029/2022gl100091

The Matplotlib Development Team. (2023). Matplotlib: Visualization with Python (v3.8.2). [Software]. *Zenodo*. https://doi.org/10.5281/zenodo.10150955

The NCAR Command Language. (2019). UCAR/NCAR/CISL/TDD. (Version6.6.2). [Software]. https://doi.org/10.5065/D6WD3XH5

Tilmes, S., Richter, J. H., Mills, M. J., Kravitz, B., MacMartin, D. G., Garcia, R. R., et al. (2018). Effects of different stratospheric SO_2 tion altitudes on stratospheric chemistry and dynamics. *Journal of Geophysical Research: Atmospheres*, *123*(9), 4654–4673. https://doi.org/10.1002/2017JD028146

Todt, M. A., Asher, E., Hall, E., Cullis, P., Jordan, A., Xiong, K., et al. (2023). Baseline Balloon Stratospheric Aerosol Profiles (B2SAP)—Systematic measurements of aerosol number density and size. *Journal of Geophysical Research*, *128*(12), e2022JD038041. https://doi.org/10.1029/2022JD038041

Toon, O. B., Turco, R. P., Westphal, D., Malone, R., & Liu, M. (1988). A multidimensional model for aerosols: Description of computational analogs. *Journal of the Atmospheric Sciences*, *45*(15), 2123–2144. https://doi.org/10.1175/1520-0469(1988)045<2123:ammfad>2.0.co;2

Vömel, H., Evan, S., & Tully, M. (2022). Water vapor injection into the stratosphere by Hunga Tonga-Hunga Ha'apai. *Science*, *377*(6613), 1444–1447. https://doi.org/10.1126/science.abq2299

Wrana, F., Niemeier, U., Thomason, L. W., Wallis, S., & von Savigny, C. (2023). Stratospheric aerosol size reduction after volcanic eruptions. *Atmospheric Chemistry and Physics*, *23*(17), 9725–9743. https://doi.org/10.5194/acp-23-9725-2023

Xu, J., Li, D., Bai, Z., Tao, M., & Bian, J. (2022). Large amounts of water vapor were injected into the stratosphere by the Hunga Tonga–Hunga Ha'apai Volcano Eruption. *Atmosphere*, *13*(6), 912. https://doi.org/10.3390/atmos13060912

Yu, P., Davis, S. M., Toon, O. B., Portmann, R. W., Bardeen, C. G., Barnes, J. E., et al. (2021). Persistent stratospheric warming due to 2019–2020 Australian wildfire smoke. *Geophysical Research Letters*, *48*(7), e2021GL092609. https://doi.org/10.1029/2021GL092609

Yu, P., Portmann, R. W., Peng, Y., Liu, C.-C., Zhu, Y., Asher, E., et al. (2023). Radiative forcing from the 2014 to 2022 volcanic and wildfire injections. *Geophysical Research Letters*, *50*(13), e2023GL103791. https://doi.org/10.1029/2023GL103791

Yu, P., Toon, O. B., Bardeen, C. G., Mills, M. J., Fan, T., English, J. M., & Neely, R. R. (2015). Evaluations of tropospheric aerosol properties simulated by the community earth system model with a sectional aerosol microphysics scheme. *Journal of Advances in Modeling Earth Systems*, *7*(2), 865–914. https://doi.org/10.1002/2014ms000421

Yu, P., Toon, O. B., Bardeen, C. G., Zhu, Y., Rosenlof, K. H., Portmann, R. W., et al. (2019). Black carbon lofts wildfire smoke high into the stratosphere to form a persistent plume. *Science*, *365*(6453), 587–590. https://doi.org/10.1126/science.aax1748

Yuen, D. A., Scruggs, M. A., Spera, F. J., Zheng, Y., Hu, H., McNutt, S. R., et al. (2022). Under the surface: Pressure-induced planetary-scale waves, volcanic lightning, and gaseous clouds caused by the submarine eruption of Hunga Tonga-Hunga Ha'apai volcano. *Earthquake Research Advances*, *2*(3), 100134. https://doi.org/10.1016/j.eqrea.2022.100134

Zhu, Y., Bardeen, C. G., Tilmes, S., Mills, M. J., Wang, X., Harvey, V. L., et al. (2022). Perturbations in stratospheric aerosol evolution due to the water-rich plume of the 2022 Hunga-Tonga eruption. *Commun Earth Environ*, *3*(1), 248. https://doi.org/10.1038/s43247-022-00580-w

Zhu, Y., Toon, O. B., Jensen, E. J., Bardeen, C. G., Mills, M. J., Tolbert, M. A., et al. (2020). Persisting volcanic ash particles impact stratospheric SO_2 lifetime and aerosol optical properties. *Nature Communications*, *11*(1), 4526. https://doi.org/10.1038/s41467-020-18352-5